Research Article | Vol. 10, No. 11 / 1 November 2019 / Biomedical Optics Express 5639
Biomedical Optics EXPRESS

Proper measurement of pure dielectrophoresis force acting on a RBC using optical tweezers

MEHRZAD SASANPOUR, ALI AZADBAKHT, PARISA MOLLAEI, AND S. NADER S. REIHANI*

Department of Physics, Sharif University of Technology, Tehran, Iran
**Corresponding author: sreihani@sharif.edu*

Abstract: The force experienced by a neutral dielectric object in the presence of a spatially non-uniform electric field is referred to as dielectrophoresis (DEP). The proper quantification of DEP force in the single-cell level could be of great importance for the design of high-efficiency micro-fluidic systems for the separation of biological cells. In this report we show how optical tweezers can be properly utilized for proper quantification of DEP force experienced by a human RBC. By tuning the temporal frequency of the applied electric field and also performing control experiments and comparing our experimental results with that of theoretically calculated, we show that the measured force is a pure DEP force. Our results show that in the frequency range of 0.1-3 MHz the DEP force acting on RBC is frequency independent.

1. Introduction

Dielectrophoresis [DEP], discovered by Pohl [1], is referred to the electric interaction between a dielectric object and an External Spatially Non-uniform Electric field (ESNE). The non-zero net dipole moment of the object induced by the ESNE is responsible for this interaction [2,3]. DEP is mainly observed in the micro-scale, in which a pattern of micro-electrodes produces the ESNE inside the sample chamber [4]. Normally the electrodes are printed on the chamber wall. A dielectric object present in the vicinity of the micro-electrodes would experience a DEP force, either towards the electrodes or away from them depending on the contrast between the electrical properties of the object and the surrounding medium [2,3]. It is shown that the magnitude of the DEP force is a linear function of the intensity gradient of the electric field present at the position of the object [2,3]. A variety of micro-electrode configurations have been used for producing a desired spatial gradient of the electric field [4]. DEP has been an indispensable technique in many biomedical researches at different concentration levels, from single cell to bulk concentrations [5–10]. At the bulk level, for instance, DEP is utilized for sorting of biological cells based on their electrical and physical properties [5,6]. Such a sorting technique has been used as a diagnostic process for different diseases [6,7]. This cell separation technique is shown to be effective even at very low concentrations of the target cells inside the biological compounds [8]. As an example, Circulating Tumor Cells (CTCs), which are known to be the key elements in the progression of cancers, could be separated from blood utilizing DEP along with a Field Flow Fractionation (DEP-FFF). Note that CTCs are very rarely found in the blood [8]. In the single-cell level, DEP is widely used for investigation on the electrical and mechanical properties of biological cells [9,10]. Utilizing DEP in the single-cell-level investigation would be of great importance as it can lead to a deep electrical and structural knowledge about the cell of interest. Yet, such a knowledge can be used for improving the separation efficiency in the bulk-level, as well [11]. One approach in this regard would be utilizing Optical Tweezers (OT) alongside the DEP setup [12–16]. One goal for such a combination would be not only performing manipulation on the cell of interest, but also measuring the magnitude of DEP force experienced by the cell [17,18], as OT can precisely measure an external force in the range of tens of femto-Newton up to few nano-Newton [19]. Though such a combination is previously used with the goal of discriminating between human

#374959 https://doi.org/10.1364/BOE.10.005639
Journal © 2019 Received 13 Aug 2019; revised 23 Sep 2019; accepted 4 Oct 2019; published 10 Oct 2019

Biomedical Optics EXPRESS

Red Blood Cell (RBC) at different ages [18], however, the method utilized for quantification of the DEP force was not accurate enough. This is because in the mentioned work the RBC of interest was directly trapped at the focus of the laser beam and the force was measured using the calibration parameters extracted by the calibration [20] of the Brownian movement of the trapped cell. Utilizing OT in this way would not lead to an accurate force measurement for two reasons: 1) In the power spectrum calibration method [20] it is assumed that the trapped object is a rigid sphere [20,21]. Considering the flexible "discocyte" shape of RBC with a very large aspect ratio of ~ 4 the obtained calibration parameters could not be accurate. 2) In the process of measuring the external force using OT one essential key is that the shape of the handle trapped by OT remains unchanged as a slight change in the shape of the handle could significantly change the calibration parameters [20]. Therefore, RBC itself may not be used as a handle for force spectroscopy due to its flexible nature. In this work, we show how an external DEP force can be accurately measured by OT. More specifically, we attached a solid micron-sized Polystyrene (PS) bead to the cell's structural wall. Performing calibration process before attachment allows for very accurate measurement of the DEP force experienced by the cell of interest.

Consider the case where a spherical dielectric object suspended inside an aqueous medium and subjected to an ESNE. Due to the presence of the electric field several type of forces can be acting on the object. Electro-Phoresis (EP) is referred to the motion of an object with a non-zero net electric charge under an external electric field [11,22]. In the DC and low frequency AC electric field, this electrokinetic force can lead to a translational movement of the object [11,22]. Even if the object of interest has no net electric charge, the force acting on the ions inside the liquid can exert a drag force on the object.

Electro-Osmosis (EO) refers to the movement of the aqueous medium containing ions [23]. This force is mainly seen when the electrodes utilized for producing the ESNE are immersed into the liquid, in which case an Electric Double Layer (EDL) forms next to the electrodes [23]. Interaction between the tangential component of the electric field and the EDL causes a vortical movement of the liquid [23,24]. Such a movement in the liquid can exert a drag force on the object suspended therein [11,22]. It should be noted that EO occurs for time varying electric fields and is strongly frequency-dependent [23].

According to the Helmholtz-Smoluchowski equation [25], for an object suspended in an ionic solution the EO and EP-induced solution velocity and the resulted forces can be written as:

$$\vec{v}_{eo} = \mu_{eo}\vec{E} = -\frac{\varepsilon_m \zeta_{eo}}{\eta}\vec{E} \quad ; \quad \vec{F}_{eo,drag} = 6\pi\eta r\vec{v}_{eo} \tag{1}$$

$$\vec{v}_{ep} = \mu_{ep}\vec{E} = -\frac{\varepsilon_m \zeta_{ep}}{\eta}\vec{E} \quad ; \quad \vec{F}_{ep,drag} = 6\pi\eta r\vec{v}_{ep} \tag{2}$$

where μ_{eo} and μ_{ep}, respectively, are EO and EP-induced mobility, ε_m is the electrical permittivity of the solution. ζ_{eo} (ζ_{ep}) represents zeta potential at the shear plane of EDL near the electrodes (charged particle). η and r, respectively, are viscosity of the medium, and radius of the spherical object.

In case the electric field experienced by the object is spatially non-uniform the DEP force experienced by the object can be written as below in the dipole moment approximation [26]

$$\vec{F}_{DEP} = 2\pi r^3 \varepsilon_m Re[K(\omega)]\nabla E^2 \tag{3}$$

where ω, E, r, and ε_m, represent frequency, amplitude of the electric field, radius of the object, and electrical permittivity of the surrounding medium, respectively. $K(\omega)$ denotes the Clausius-Mossotti (CM) factor given by $K(\omega) = \dfrac{\varepsilon_p^* - \varepsilon_m^*}{\varepsilon_p^* + 2\varepsilon_m^*}$ with ε_p^* and ε_m^* being the complex electrical permittivity of the particle and medium, respectively. ε^* for each medium can be written as

Biomedical Optics EXPRESS

$\varepsilon^* = \varepsilon - i\frac{\sigma}{\omega}$ with ε and σ being the electrical permittivity and conductivity of the medium. Note that the force depends on the spatial gradient of the electric field intensity (∇E^2) not the electric field itself, and that the CM factor is a frequency dependent parameter with a possibility of being positive or negative [2,3]. Due to presence of electric field intensity gradient in the vicinity of the electrodes, the object would be either pulled towards or pushed away from the electrodes, respectively, for positive and negative CM factor values. Very often the positive and negative values of CM factor are referred to as nDEP and pDEP, respectively [2,3].

In order to calculate the DEP force exerted on an object with a desired shape one has to calculate the CM factor for the object as well as the intensity gradient at the position of the object. The electric field intensity can be calculated by solving the Laplace equation in the space between the electrodes in the absence of the object. In order to calculate the CM factor one has to, first, calculate the electric field around the object by solving the Laplace equation for the case when the dielectric object is subjected to a constant external electric field (performed in the above step). Next, the calculated electric field is compared with that of produced by a single electric dipole, from which the CM factor can be read-off. Note that the CM factor can be calculated for objects with different shapes. For a RBC modeled as a double concentric ellipsoid, for instance, the CM factor for each direction ($K_i(w)$, with $i = x, y, z$) can be given by [27]

$$
\begin{aligned}
K_i(w) &= \frac{1}{3}\frac{\left(\varepsilon^*_{mem} - \varepsilon^*_m\right) + 3X_i\rho\left(\varepsilon^*_{mem} + A_{2i}\left(\varepsilon^*_m - \varepsilon^*_{mem}\right)\right)}{\varepsilon^*_m + A_{2i}\left(\varepsilon^*_{mem} - \varepsilon^*_m\right) + 3X_i\rho A_{2i}\left(1 - A_{2i}\right)\left(\varepsilon^*_{mem} - \varepsilon^*_m\right)} \\
X_i &= \frac{1}{3}\frac{\left(\varepsilon^*_{cyto} - \varepsilon^*_{mem}\right)}{\varepsilon^*_{mem} + A_{1i}\left(\varepsilon^*_{cyto} - \varepsilon^*_{mem}\right)} \\
A_{1i} &= \frac{a_1a_2a_3}{2}\int_0^\infty \frac{ds}{\left(s + a_i^2\right)\sqrt{\left(s + a_1^2\right)\left(s + a_2^2\right)\left(s + a_3^2\right)}} \\
A_{2i} &= \frac{\left(a_1 + d\right)\left(a_2 + d\right)\left(a_3 + d\right)}{2}\times \\
&\int_0^\infty \frac{ds}{\left(s + \left(a_i + d\right)^2\right)\sqrt{\left(s + \left(a_1 + d\right)^2\right)\left(s + \left(a_2 + d\right)^2\right)\left(s + \left(a_3 + d\right)^2\right)}} \\
\rho &= \frac{a_1a_2a_3}{\left(a_1 + d\right)\left(a_2 + d\right)\left(a_3 + d\right)} \\
F_{DEP,i} &= 2\pi a_1a_2a_3\varepsilon_m\frac{d}{dx_i}\sum_{j=1}^{3}\left(Re\left[K_j(\omega)\right]E_j^2\right)
\end{aligned}
\tag{4}
$$

where A_{1i}, and A_{2i} are depolarization factor of the ellipsoids for i direction. It is worth mentioning that A_{1i} and A_{2i} could be considered equal as the shell defined by the two ellipsoids, d, is very thin [28]. X_i denotes the effective dipole factor for the inner ellipsoid of RBC. ε_{cyto}, ε_{mem}, and ε_m, are electrical permittivity of the cytoplasm, membrane, and medium, respectively. ρ defines the volume ratio between the two ellipsoids (defined by diameters of (a_1, a_2, a_3) and (($a_1 + d$), ($a_2 + d$), ($a_3 + d$)). The electrical permittivity and conductivity of RBC are obtained from [28].

Depending on the temporal and spatial frequency of the electric field, either of above mentioned forces can contribute to the net force acting on the object [22,23]. Though, producing a pure DEP force is always a challenge [11,12], however, it is still possible to minimize the contribution from the forces other than DEP force [11,12,23]. For instance, EP-induced force can be neglected if the object has no net electric charge or the frequency of the electric field is considerably large [11,22].

Biomedical Optics EXPRESS

It is also shown that EO effect can also be suppressed by increasing the temporal frequency of the electric field [23].

2. Material and methods

Our home-designed dual trap OT is schematically shown in Fig. 1(a), which consists of one fixed and one movable trap. Note that the fixed trap is used for force measurement in the current research. A continuous wave laser source (Nd:YAG, λ=1064nm, Coherent) is expanded via a beam expander to slightly overfill the back aperture of a high Numerical Aperture (NA) objective lens (UPlanSAPo, 60×, Water, NA=1.2, Olympus). The laser beam is then focused by the objective into the sample chamber, which consists of a microscope slide and a coverslip. A small parafilm sheet with a square opening with a side of ~5 mm was used as spacer between the glass walls.The microscope slide contained two long parallel gold micro-electrodes (schematically shown in the blown-up view of the sample chamber) in order to produce the ESNE required for this measurement. It should be mentioned that the vertical and transverse distances of the nearest electrode from the focus were, respectively, about10μm and 2.5μm. This means that, first, the presence of the electrodes on the microscope slide does not influence the quality of the trap as they are located after the focus along the optical pathway of the trapping beam. This can be easily seen from the symmetric shape of the optical potential well shown in the inset of Fig. 1(c). Second, a simple calculation based on the propagation of the Gaussian beams show that only edge of the trapping beam touches the nearest electrode. Figure 1(b) shows real photograph of electrodes (three pairs) coated on a microscope slide using photo-lithography [4]. Each electrode contains a layer of gold (Au) with a thickness of ~100 nm on top of a layer of Chrome (Cr) with a thickness of ~10 nm. A function generator (OWON AG 2025F, 50 MHz) was used for applying the required voltage difference to the electrodes. Once a bead is trapped in the focus of OT, the light passing through the chamber (including the un-scattered or direct light and the scattered from the trapped bead) is collected by means of a condenser lens. The collected light is then reflected-off the optical pathway of the microscope by means of a dichroic mirror impinging a Quadrant Photo Diode (QPD) (S5981, Hamamatsu). The output voltages of the QPD was digitized and then used for calculating the precise position of the bead inside the optical trap. The visualization of the sample was performed by means of a CMOS camera (puA1280-54um, Basler). In order to extract the calibration parameters of the trap the positional time series of the trapped bead was first grabbed from the QPD and then underwent a power spectrum analysis [20,29]. In this calibration method the bead is treated as a damped-harmonic oscillator externally driven by a random force (thermal noise), for which the Power Spectral Density (PSD) of the positional time series can be given by [20]:

$$P(f) = |\widetilde{x}(f)|^2 = \frac{k_B T}{\gamma \pi^2 (f_c^2 + f^2)} \tag{5}$$

where $f_c = \frac{k}{2\pi\gamma}$ with f_c, γ, and k, respectively, being the corner frequency of the trap, drag coefficient, and trap stiffness. $k_B T$ represents thermal energy accessible for the trapped bead with k_B and T, respectively, being the Boltzmann constant and absolute temperature of the environment. In each run of the experiment once a bead was trapped its positional time series were collected and then PSD of the recorded data was fitted by Eq. (5) in order to extract the trap stiffness [20]. It should be mentioned that the second calibration factor, known as voltage-to-position conversion factor ($\beta(\frac{nm}{Volt})=\frac{x}{V}$) is also used as the second fitting parameter [20]. A typical PSD for a trapped 3μm polystyrene bead is shown in Fig. 1(c), in which the solid curve shows fit to Eq. (5). Once the calibration parameters are known, any external force acting on the bead can be precisely determined. In order to do so the net displacement of the bead in the trap (in voltage) is first multiplied by β and then by k. Figure 1(d) typically shows the displacement of the trapped bead once it is subjected to the DEP force. Note that our entire measurements are based on the

Biomedical Optics EXPRESS

signal grabbed from the QPD not the camera and the camera is only used for visualization of the sample. Two types of Polystyrene (PS) beads with a mean diameter of 3μm and 282 nm were used in this research, both of which were purchased from Spherotech. The 3μm beads were coated with Anti-Digoxigenin, whereas the 282 nm beads labeled with fluorescent tags ($\lambda_{excitation}$= 488nm, $\lambda_{emission}$=500↔600nm). For the RBC related measurements a 3μm bead was attached to one end of the RBC of interest after calibration of the trap. The procedure for this attachment can be found in ref.[30]. The buffer for the RBC experiment was 9 mg/ml NaCl solution. A Leica confocal microscope (Leica TCS SPE) equipped with a dry objective (10×, NA=0.3) was used for fluorescent microscopy visualization used in this research.

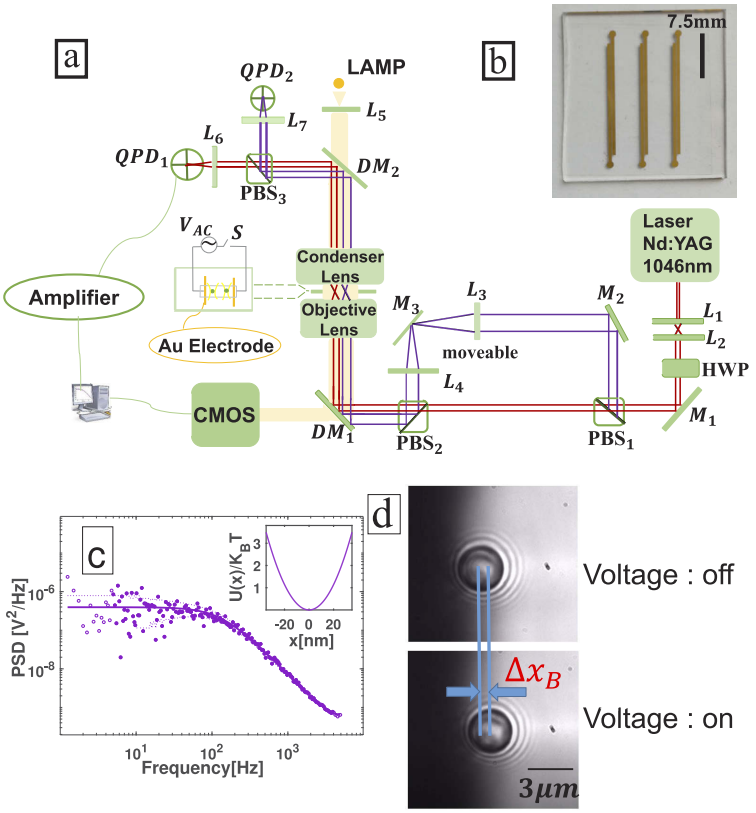

Fig. 1. (a) The schematic of OT setup including lenses (L_1-L_7), Mirror (M_1-M_3), dichroic mirrors (DM_1, and DM_2), objective and condenser lenses, $QPD_{1,2}$, amplifier and Camera. (b) Photograph of the sample chamber including the two parallel microelectrodes used for producing the ESNE. The electrodes had a width of 500μm with a lengths of 15 mm and a inter-space of 100μm. (c) A typical PSD plot of the recorded positional time series of a trapped 3μm PS bead immersed in DI water. The sampling frequency and laser power were 10 kHz and 160mW, respectively. (d) Typical visualization of the trapped bead in the presence and absence of the electric field Visualization 1. Δx_B denotes the displacement of trapped bead due to the exerted force.

Biomedical Optics EXPRESS

3. Results and discussion

3.1. Pure DEP force check

OT can only measure the total force acting on an object. In order to set a condition that only DEP force acts on the sample RBC it is crucial to minimize the EP and EO contribution to the total force. Considering that the measurement is performed at considerably larger frequencies the EP-induced force acting on the object would be zero. However, EO force induced by the ions inside the medium can still exert a drag force on the object. Therefore, in order to minimize the EO-induced force acting on the object it is crucial to find a condition, which prevents the movement of the fluid around the object. One solution for this could be increasing the temporal frequency of the external electric field [23]. In a certain range of frequencies the liquid around the object may remain still. It is previously shown that the characteristic frequency, at which the EO effect occurs is given by $\omega = (\sigma_m/\varepsilon_m)(\lambda_D/L)$, in which λ_D and L are Debye length and the typical size of the system, respectively [31]. To find this characteristic frequency the sample chamber was filled with a diluted solution of the fluorescent beads (to be used as tracers) and the sample was visualized by the confocal imaging system in the $x-z$ scan mode at different temporal frequencies of the electric field. Note that x and z directions represent the transverse and axial (perpendicular to the chamber wall) directions, respectively. The recorded time-lapsed frames at frequencies of 500 Hz, 5 kHz, and 50 kHz can be found in the Fig. 2 (see Visualization 2, Visualization 3, and Visualization 4. The final scene from each of the mentioned visualizations are presented in Fig. 2. Note that due to the movement of the liquid at low frequencies some part of the beads (green color) are moved away from the electrodes (the region shown by dashed boundary). However, at frequency of ~50 kHz the beads, and hence the fluid, stop moving. This shows that our DEP force measurement should be conducted at frequencies above 50 kHz. It should be mentioned that the $x-z$ image of a bead will rather look like a rod due to considerably larger Point Spread Function (PSF) of the imaging system in the axial direction [32]. For our case the aspect ratio of the image would be around 10. Also note that, as it is mentioned earlier, EO force is a drag-based force, whereas DEP is a volume force. In other words EO force linearly scales with the radius of the object, whereas DEP force is a function of r^3. Considering the small size of the fluorescent beads the DEP force in the current test would be much smaller (by a factor of $\sim 10^{-14}$) than EO force.

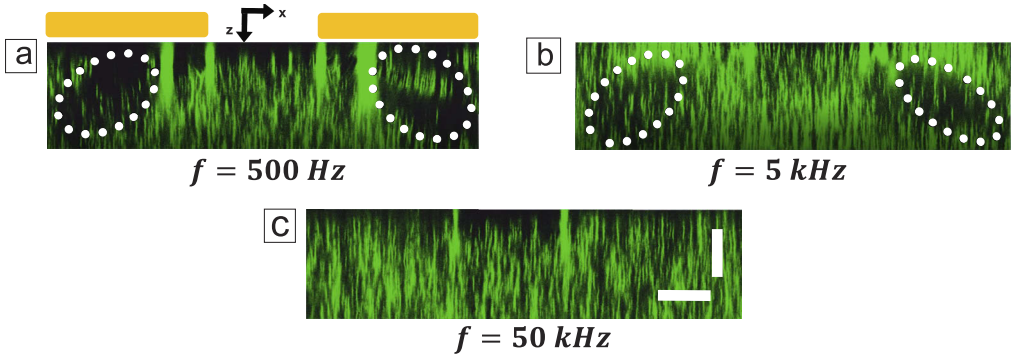

Fig. 2. Fluorescent nano particle tracers (green color) show the fluid motion under the external electric field (V_{pp}=6 V) at different frequencies (f) of (a) 500 Hz, (b) 5 kHz, and (c) 50 kHz. The vortical movement of the fluid disappeared at a frequency 50 kHz and above (data are not shown), which demonstrates the absence of EO effect (Visualization 2, Visualization 3, and Visualization 4). The scale bars in the panels a-c are 40μm.

Biomedical Optics EXPRESS

3.2. DEP force acting on a PS bead

In order to measure the DEP force exerted on a PS bead subjected to an ESNE, first, a 3μm PS bead was trapped and calibrated when the switch S (Fig. 1(a)) was open. Then the switch was closed, upon which the PS bead was displaced due to the DEP force acting on it. Figure 1(d) and also Visualization 1 typically show such a displacement. By measuring this displacement in voltage from QPD and multiplying it with the conversion factor (β) and spring constant (k) resulted from the calibration process the net force acting on the bead was measured. Note that the bead is pushed away from the electrode, which shows that the force at this particular frequency is nDEP. In order to show the force acting on the bead is a pure DEP force this measurement was repeated at different voltage differences (V) applied to the electrodes (the bead was kept in the same place), results of which are shown in Fig. 3(a). Note that as for a pure DEP force the magnitude of the force should be a linear function of V^2 as E scales linearly with V [2,3]. The solid red line in Fig. 3(a) shows a linear fit to the experimental data, which confirms the linear dependence of the measured force on V^2.The same measurement was repeated for the bead trapped at different lateral distances from one of the electrodes for a constant voltage difference, results of which are shown in Fig. 3(b). From Fig. 3(b) one can see that: (1) The force is fairly symmetric and the direction of the force changes as the bead is moved to the opposite half of the chamber. (2) The magnitude of the force is larger at the positions closer to the electrodes. This is because the gradient of electric field intensity is larger in the vicinity of the electrodes. (3) The red circles connected with a solid line show the result of simulation performed using COMSOL Multiphysics 5.3a for the similar configuration, which is in a good agreement with the experimental results. A slight difference between the experimental and simulation results at the edge positions could be due to the little roughness presented on the edges of the electrodes.

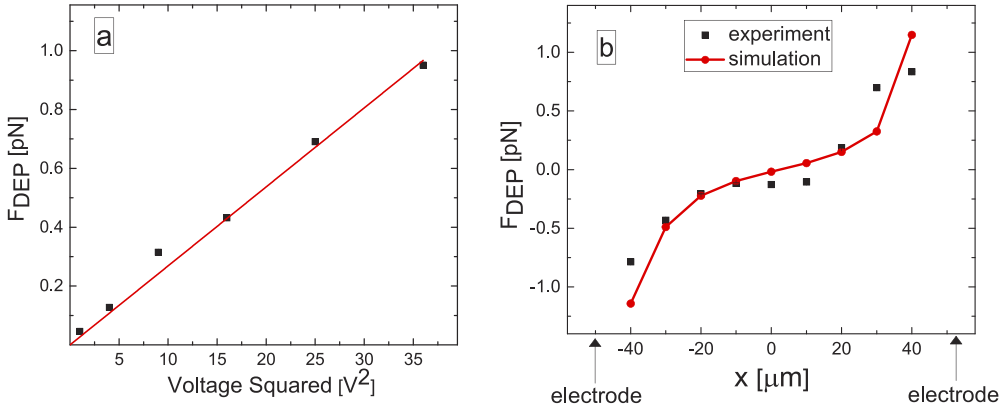

Fig. 3. Measurement of DEP force exerted on a trapped 3μm PS bead. (a) The measured DEP force as a function of squared applied voltage. The solid red line shows the linear fit ($y = \alpha x$) to the experimental data point with a result of α=0.0268±0.0006. (b) The measured DEP force as a function of lateral position of the bead from the electrodes (the middle point as reference). The red circled connected with a solid line with similar color represent results of simulation for a similar configuration. Each data point represents average over three measurement with sampling frequency of 1kHz. The standard error of the averaged data considered as error bar, which is not visible in the graphs as they are smaller than the representing symbols. The sampling duration time for (a) and (b), respectively was 2 and 1 seconds. The frequency of the external voltage source was 700 kHz and the peak-to-peak voltage difference for (b) was V_{pp}=10V.

Biomedical Optics EXPRESS

3.3. DEP force acting on a RBC

The method described above can not be directly used for measuring the DEP force acting on a RBC due to the non-spherical shape and flexibility of the cell (explained earlier) [20]. Our solution for is to measure the force exerted on a bead-RBC complex (attached together) and subtract it by that of exerted on a single trapped PS bead. Anti-Dig coated polystyrene beads are a good choice for this task as their coated protein can form a stiff chemical bond to the spectrin network of RBC. For this part of measurement we utilized both of the traps provided by our dual trap setup, however, the force measurement was still conducted by the fixed trap. The experiment started when the fixed trap was occupied by a PS bead in the vicinity of the electrode, whereas the movable other trap was occupied with a RBC and positioned far away from the bead. Once measurement of the force acting on the bead (explained in the previous section) was done the RBC was brought next to the bead. Leaving the bead and RBC in contact for a little while formed the attachment, after which the trap holding the RBC was switched off. Note that in this situation the polystyrene bead was still grabbed by the fixed trap. Applying voltage to the electrodes in this situation led to a DEP force exerted on the bead-RBC complex, which was measured using the fixed trap. Figure 4(b), which contains two frames from each of the Visualization 5 and Visualization 6 show the close view of the scenes when the external electric field is on and off. ΔX_B and ΔX_{RB} denote the displacement of the single bead and RBC-bead complex, respectively. The net DEP force exerted on the RBC was then calculated by subtracting the two measured forces. The entire force measurement procedure was repeated at different frequencies, results of which are summarized in Fig. 4(a). In this figure the black squares represent average over seven measurements on seven different RBCs, for which the standard error is shown as error bar. The results of seven individual measurements are shown in the inset. The solid red line shows the simulation result for RBC, which fairly confirms the observed behavior. Note that the measured force is rather constant in the range of 0.1-3 MHz. This is in accordance with the theoretical results, though the theory predicts a larger magnitude for the measured force. One possible reason for this could be the difference between the approximated (ellipsoid) and real (discocyte) shapes of the cell. Simulation result for a single PS bead is shown with solid blue line for comparison. We noticed that both of the bead and RBC experience a nDEP force (pushed away from the electrode). Just like the single bead case, the measurement was performed for different voltage differences applied to the electrodes to make sure that the measured force is pure DEP. The results for this measurement are presented in Fig. 4(c). Each data point of Fig. 4(c) represents average over two measurements, standard deviation of which is shown with error bar. The Red solid line shows fit to a linear function (without intercept), which fairly follows the experimental results. This confirms that the measured force is DEP-based, indeed. One could argue that the presence of the RBC in the vicinity of the bead could alter the magnitude of the DEP force experienced by either of the RBC and bead by altering the spatial distribution of the electric field.In order to check this out we performed a control experiment. In this experiment the last step of the measurement was repeated with holding the RBC next to the polystyrene bead (without being attached to it) using the movable trap (Fig. 5(a) and the Visualization 7). The measured net force in this situation (red circles in Fig. 5(b)) was compared with that of measured when the bead was attached to the RBC (blue triangles in Fig. 5(b)), and also with that of measured in the absence of the RBC (black squares in Fig. 5(b)). Note that the measured force acting on the bead in the presence and absence of the RBC is very similar (and both are considerably smaller than that of RBC-bead complex). This can rule-out the possibility that the presence of the RBC alters the DEP force experienced by the bead itself (assumed to be measured in the first step of the experiment), which confirms the validity of our method for measuring the DEP force experienced by the RBC.

Biomedical Optics EXPRESS

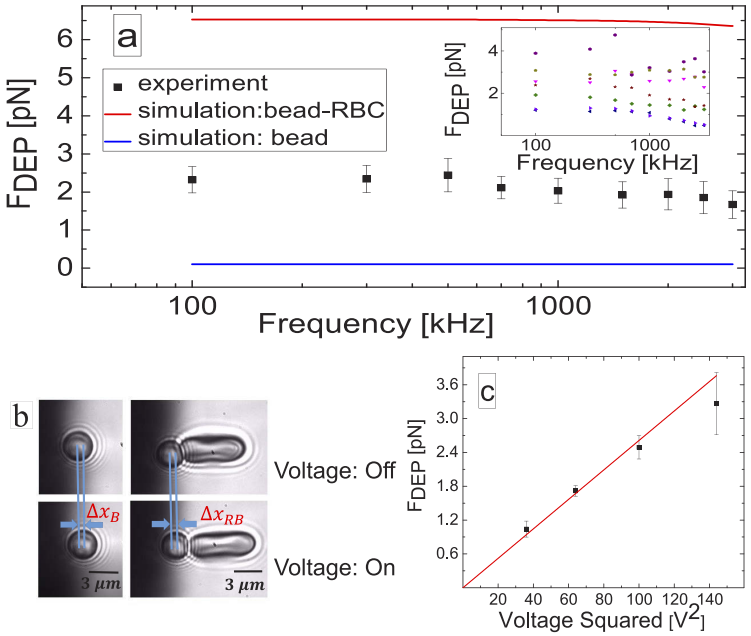

Fig. 4. (a) The measured DEP force exerted on RBC-bead complex as a function of frequency with $V_{pp} = 12V$. Each data point represents average over seven different measurements, which are individually presented in the inset. The solid red and blue lines, respectively, show theoretically calculated DEP force acting on the RBC-bead complex, and the bead alone. In this calculation a_1, a_2, and a_3 values considered to be 3.8μm, 1.2 μm, and 3.2μm, respectively. The thickness of the cell membrane was considered to be d =4.5 nm. The electrical parameters of the medium and polystyrene was considered as σ_m=1.1S/m, ε_m= 75ε_0, σ_{ps}=0.0025S/m, and ε_{ps}=2.55ε_0. (b) The visualization of the scene when a single bead (left column) and bead-RBC complex (right column) are subjected to a DEP force. Δx_B, and Δx_{RB} denote the displacement of the single bead and RBC-bead complex respectively, when the voltage is applied to the electrodes (Visualization 5 and Visualization 6). (c) The net DEP force experienced by the RBC as a function of voltage squared at a frequency of 2 MHz. The red solid line represents fit to linear function of $y = \alpha x$ with the result of α=0.0261±0.0008

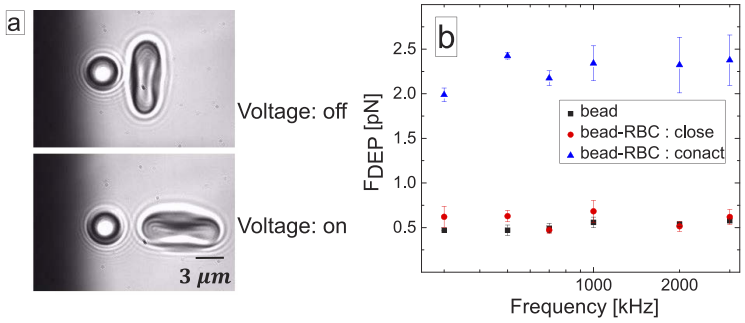

Fig. 5. (a) The visual appearance of a bead and a RBC are kept by separate traps. The upper and lower images are taken when the switch is off and on, respectively (Visualization 7). (b) The measured net force acting on the bead at different conditions: The bead is attached to the RBC (blue triangles), the bead is close to the RBC but not attached (red circles), and the RBC is far away from the bead (black squares). The data points show average over two data sets with $V_{pp} = 8V$.

Biomedical Optics EXPRESS

4. Conclusion

DEP force is widely used for separation of biological cells in micro-fluidic systems. Despite the great effort in this regard very few report on the quantification of DEP force in the single-cell level can be found in the literature. OT are known as indispensable tools for force spectroscopy. In this work we show how OT can be used for proper measurement of the DEP force acting on a RBC. In order to do so we attach a micro-scale bead to the cell to be used as a handle to be trapped by OT. By measuring the force acting on the RBC-bead complex and subtracting it by the force acting on a single bead we were able to measure the DEP force experienced by the RBC. By checking the fingerprints of DEP force and also performing control experiment we have shown that the force measured in our experimental condition is pure DEP. Our theoretical and experimental results show that in the temporal frequency range of 0.1-3 MHz the DEP force exerted on a single RBC is frequency independent.

Funding

Sharif University of Technology (G930208).

Disclosures

The authors declare that there are no conflicts of interest related to this article.

References

1. H. A. Pohl, "The motion and precipitation of suspensoids in divergent electric fields," J. Appl. Phys. **22**(7), 869–871 (1951).
2. P. R. C. Gascoyne and J. Vykoukal, "Particle separation by dielectrophoresis," Electrophoresis **23**(13), 1973–1983 (2002).
3. R. Pethig, "Review article dielectrophoresis: Status of the theory," Biomicrofluidics **4**(2), 022811 (2010).
4. M. Li, W. H. Li, J. Zhang, G. Alici, and W. Wen, "A review of microfabrication techniques and dielectrophoretic microdevices for particle manipulation and separation," J. Phys. D: Appl. Phys. **47**(6), 063001 (2014).
5. T. Z. Jubery, S. K. Srivastava, and P. Dutta, "Dielectrophoretic separation of bioparticles in microdevices: A review," Electrophoresis **35**(5), 691–713 (2014).
6. H. Li and R. Bashir, "Dielectrophoretic separation and manipulation of live and heat-treated cells of Listeria on microfabricated devices with interdigitated electrodes," Sens. Actuators, B **86**(2-3), 215–221 (2002).
7. F. F. Becker, X. B. Wang, Y. Huang, R. Pethig, J. Vykoukal, and P. R. Gascoyne, "Separation of human breast cancer cells from blood by differential dielectric affinity," Proc. Natl. Acad. Sci. **92**(3), 860–864 (1995).
8. R. C. Gascoyne and S. Shim, "Isolation of circulating tumor cells by dielectrophoresis," Cancers **6**(1), 545–579 (2014).
9. Y. J. Lo, Y. Y. Lin, U. Lei, M. S. Wu, and P. C. Yang, "Measurement of the Clausius-Mossotti factor of generalized dielectrophoresis," Appl. Phys. Lett. **104**(8), 083701 (2014).
10. E. Du, M. Dao, and S. Suresh, "Quantitative biomechanics of healthy and diseased human red blood cells using dielectrophoresis in a microfluidic system," Extreme Mech. Lett. **1**, 35–41 (2014).
11. M. A. Saucedo-Espinosa, M. M. Rauch, A. LaLonde, and B. H. Lapizco-Encinas, "Polarization behavior of polystyrene particles under direct current and low-frequency ($<1kHz$) electric fields in dielectrophoretic systems," Electrophoresis **37**(4), 635–644 (2016).
12. M. T. Wei, J. Junio, and H. D. Ou-Yang, "Direct measurements of the frequency-dependent dielectrophoresis force," Biomicrofluidics **3**(1), 012003 (2009).
13. Y. Hong, J. W. Pyo, S. H. Baek, S. W. Lee, D. S. Yoon, K. No, and B. M. Kim, "Quantitative measurements of absolute dielectrophoretic forces using optical tweezers," Opt. Lett. **35**(14), 2493–2495 (2010).
14. H. Park, M. T. Wei, and H. D. Ou-Yang, "Dielectrophoresis force spectroscopy for colloidal clusters," Electrophoresis **33**(16), 2491–2497 (2012).
15. I. S. Park, S. H. Park, D. S. Yoon, S. W. Lee, and B. M. Kim, "Direct measurement of the dielectrophoresis forces acting on micro-objects using optical tweezers and a simple microfluidic chip," Appl. Phys. Lett. **105**(10), 103701 (2014).
16. G. Pesce, G. Rusciano, G. Zito, and A. Sasso, "Simultaneous measurements of electrophoretic and dielectrophoretic forces using optical tweezers," Opt. Express **23**(7), 9363–9368 (2015).
17. I. S. Park, S. H. Park, S. W. Lee, D. S. Yoon, and B. M. Kim, "Quantitative characterization for dielectrophoretic behavior of biological cells using optical tweezers," Appl. Phys. Lett. **104**(5), 053701 (2014).
18. H. J. Jeon, H. Lee, D. S. Yoon, and B. M. Kim, "Dielectrophoretic force measurement of red blood cells exposed to oxidative stress using optical tweezers and a microfluidic chip," Biomed. Eng. Lett. **7**(4), 317–323 (2017).

Biomedical Optics EXPRESS

19. A. Ashkin, J. M. Dziedzic, J. E. Bjorkholm, and S. Chu, "Observation of a single-beam gradient force optical trap for dielectric particles," Opt. Lett. **11**(5), 288–290 (1986).
20. M. Capitanio, G. Romano, R. Ballerini, M. Giuntini, F. S. Pavone, D. Dunlap, and L. Finzi, "Calibration of optical tweezers with differential interference contrast signals," Rev. Sci. Instrum. **73**(4), 1687–1696 (2002).
21. I. M. Tolić-Nørrelykke, K. Berg-Sørensen, and H. Flyvbjerg, "MatLab program for precision calibration of optical tweezers," Comput. Phys. Commun. **159**(3), 225–240 (2004).
22. M. A. Saucedo-Espinosa and B. H. Lapizco-Encinas, "Design of insulator-based dielectrophoretic devices: Effect of insulator posts characteristics," J. Chromatogr. A **1422**, 325–333 (2015).
23. N. G. Green, A. Ramos, A. González, H. Morgan, and A. Castellanos, "Fluid flow induced by nonuniform ac electric fields in electrolytes on microelectrodes. I. Experimental measurements," Phys. Rev. E **61**(4), 4011–4018 (2000).
24. A. Ramos, H. Morgan, N. G. Green, and A. Castellanos, "The role of electrohydrodynamic forces in the dielectrophoretic manipulation and separation of particles," J. Electrost. **47**(1-2), 71–81 (1999).
25. A. Ramos, H. Morgan, N. G. Green, and A. Castellanos, "AC electric-field-induced fluid flow in microelectrodes," J. Colloid Interface Sci. **217**(2), 420–422 (1999).
26. H. Nili and N. G. Green, "Higher-order dielectrophoresis of nonspherical particles," Phys. Rev. E **89**(6), 063302 (2014).
27. M. Castellarnau, A. Errachid, C. Madrid, A. Juarez, and J. Samitier, "Dielectrophoresis as a tool to characterize and differentiate isogenic mutants of Escherichia coli," Biophys. J. **91**(10), 3937–3945 (2006).
28. Y. Qiang, J. Liu, and E. Du, "Dynamic fatigue measurement of human erythrocytes using dielectrophoresis," Acta Biomater. **57**, 352–362 (2017).
29. S. M. Mousavi, S. N. S. Reihani, G. Anvari, M. Anvari, H. G. Alinezhad, and M. R. R. Tabar, "Stochastic analysis of time series for the spatial positions of particles trapped in optical tweezers," Sci. Rep. **7**(1), 4832 (2017).
30. V. Sheikh-Hasani, M. Babaei, A. Azadbakht, H. Pazoki-Toroudi, A. Mashaghi, A. A. Moosavi-Movahedi, and S. N. S. Reihani, "Atorvastatin treatment softens human red blood cells: an optical tweezers study," Biomed. Opt. Express **9**(3), 1256–1261 (2018).
31. N. Green, A. Ramos, A. González, H. Morgan, and A. Castellanos, "Fluid flow induced by nonuniform ac electric fields in electrolytes on microelectrodes. III. Observation of streamlines and numerical simulation," Phys. Rev. E **66**(2), 026305 (2002).
32. N Lukas and B. Hecht, *Principles of Nano-optics* (Cambridge University Press, 2012), Chap. 4.